Supporting Information

for

Predicting the Contribution of Chloramines to Contaminant Decay during UV/Hydrogen Peroxide Advanced Oxidation Process (AOP) Treatment for Potable Reuse

Zhong Zhang[1], Yi-Hsueh Chuang[1], Nan Huang[2], and William A. Mitch[1,*]

[1] Department of Civil and Environmental Engineering, Stanford University, 473 Via Ortega, Stanford, California 94305, United States

[2] Environmental Simulation and Pollution Control State Key Joint Laboratory, State Environmental Protection Key Laboratory of Microorganism Application and Risk Control (SMARC), School of Environment, Tsinghua University, Beijing, 100084, PR China

31 pages
5 Texts
6 Tables
12 Figures

Table of Contents

Text S1: Additional materials and methods

Materials: Sodium hypochlorite (5.65-6%) and hydrogen peroxide (30% v/v) were purchased from Fisher Scientific. 1,4-Dioxane (99.8%) was purchased from Acros Organics (Geel, Belgium). 1,4-Dioxane-d8 (99%) was purchased from Sigma-Aldrich (St. Louis, MO). All chemicals were used as received.

1,4-Dioxane analytical methods: Water samples (40 mL) were spiked with 50 μg/L 1,4-dioxane-d8 as an internal standard. The samples were then extracted vigorously with 3 mL methyl tert-butyl-ether (MtBE) for 2 min and further concentrated by nitrogen blowdown to 0.5 mL. The MtBE extract was analyzed by an Agilent 6890N gas chromatography coupled with a HP-5MS column (Agilent, CA) and a 5973N MS.

Table S1: Basic water quality data for RO permeate samples.

Sample	Chlorine residual (mg/L as Cl_2)	NH_2Cl (mg/L as Cl_2)	$NHCl_2$ (mg/L as Cl_2)	pH	TOC (mg/L)	UV_{254} (cm^{-1})	DO (mg/L)	Cl^- (mg/L)	NO_3^- (mg/L as N)	HCO_3^- (mM)
Facility 1, Event 1	3.3	2.0	1.3	5.7	0.21	0.0149	5.1	6.5	1.16	NM
Facility 1, Event 2	5.1	3.0	2.1	5.6	0.33	0.02	4.7	NM	NM	0.08
Facility 2	3.8	2.5	1.3	5.8	NM	0.012	NM	5.3	0.95	0.11

NM = Not Measured

Text S2: Modeling

Kinetic modeling was performed as described previously[1-5] using the computer program Kintecus 4.55.[4] Table S2 provides the reactions implemented for model 1 in Figure 1, based on Patton et al.[6, 7]

Table S2: Principal reactions of the UV/chloramines AOP obtained from Patton et al.[6,7]

S1	$NH_2Cl + \bullet Cl \rightarrow \bullet NHCl + Cl^- + H^+$	1.0×10^8 - 1.0×10^9 $M^{-1}s^{-1}$ (1.0×10^9 $M^{-1}s^{-1}$ in our study)
S2	$NH_2Cl + \bullet OH \rightarrow \bullet NHCl + H_2O$	5.8×10^8 $M^{-1}s^{-1}$ (1.02×10^9 $M^{-1}s^{-1}$ in our study)
S3	$NH_2Cl + \bullet Cl_2^- \rightarrow \bullet NHCl + 2Cl^- + H^+$	1.14×10^7 $M^{-1}s^{-1}$
S4	$NHCl_2 + \bullet OH \rightarrow NCl_2\bullet + H_2O$	2.6×10^8 $M^{-1}s^{-1}$ (6.21×10^8 $M^{-1}s^{-1}$ in our study)
S5	$NHCl_2 + \bullet Cl_2^- \rightarrow NCl_2\bullet + 2Cl^- + H^+$	4.4×10^6 $M^{-1}s^{-1}$
S6	$\bullet Cl + Cl^- \rightarrow Cl_2\bullet^-$	6.50×10^9 $M^{-1}s^{-1}$ (8.00×10^9 $M^{-1}s^{-1}$ in our study)
S7	$\bullet Cl + H_2O \rightarrow ClOH\bullet^- + H^+$	2.50×10^5 s^{-1}
S8	$Cl_2\bullet^- + H_2O \rightarrow Cl^- + HClOH$	1.30×10^3 s^{-1}
S9	$ClOH\bullet^- \rightarrow Cl^- + \bullet OH$	6.10×10^9 s^{-1}
S10	$HClOH \rightarrow ClOH\bullet^- + H^+$	1.00×10^8 s^{-1}
S11	$\bullet Cl + OH^- \rightarrow ClOH\bullet^-$	3.0×10^9 $M^{-1}s^{-1}$
S12	$\bullet OH + Cl^- \rightarrow ClOH\bullet^-$	4.30×10^9 $M^{-1}s^{-1}$
S13	$ClOH\bullet^- + H^+ \rightarrow H_2O + \bullet Cl$	2.10×10^{10} $M^{-1}s^{-1}$
S14	$Cl_2\bullet^- + OH^- \rightarrow ClOH\bullet^- + Cl^-$	4.50×10^7 $M^{-1}s^{-1}$
S15	$\bullet NH_2 + O_2 \rightarrow NH_2O_2\bullet$	1.2×10^8 $M^{-1}s^{-1}$
S16	$\bullet OH + H_2CO_3 \rightarrow CO_3\bullet^- + H_2O + H^+$	1.00×10^6 $M^{-1}s^{-1}$
S17	$\bullet OH + HCO_3^- \rightarrow CO_3\bullet^- + H_2O$	8.60×10^6 $M^{-1}s^{-1}$
S18	$\bullet OH + CO_3^{2-} \rightarrow CO_3\bullet^- + OH^-$	3.90×10^8 $M^{-1}s^{-1}$
S19	1,4-dioxane + $\bullet Cl \rightarrow$ product	4.4×10^6 $M^{-1}s^{-1}$
S20	1,4-dioxane + $\bullet Cl_2^- \rightarrow$ product	3.3×10^6 $M^{-1}s^{-1}$
S21	1,4-dioxane + $\bullet OH \rightarrow$ product	3.1×10^9 $M^{-1}s^{-1}$

The model derived in this manuscript contains 94 reactions obtained from the literature or from our experimental results. Table S3 tabulates the principal reactions. This model is based upon the model of Chuang et al.[3]. Updates to this base model include: 1) an updated quantum yield for NH_2Cl photolysis (0.35 vs. 0.2) in equation S22), 2) incorporation of $NHCl_2$ photolysis with an associated quantum yield (0.75 in equation S23), 3) addition of newly measured reaction rate constants with $NHCl_2$ (equation S29) and DOC (equation S54), 4) reactions S32-45 associated with $\bullet NH_2$ and •NHCl, and 5) addition of reactions with carbonate species (equations S109-S115).

Table S3: Principal reactions in the kinetic model

No.	Reaction	Rate constant	Reference
Photolysis reactions			
S22	$NH_2Cl \xrightarrow{h\nu} \bullet NH_2 + \bullet Cl$	$r_{radical} = \frac{E_P^0[1-10^{-\varepsilon Cd}]\cdot\Phi}{d}$	5
S23	$NHCl_2 \xrightarrow{h\nu} \bullet NHCl + \bullet Cl$	E_P^0: photon flux at 254 nm (mEinstein s^{-1} cm^{-2})	
S24	$H_2O_2 \xrightarrow{h\nu} \bullet OH + \bullet OH$	d: pathlength (cm)	
S25	$HO_2^- \xrightarrow{h\nu} \bullet OH + O\bullet^-$	ε: molar extinction coefficient	
		Φ: quantum yield (mol/Einstein)	
		C: concentration of oxidant	
Oxidant scavenging reactions			
S26	$NH_2Cl + \bullet OH \rightarrow \bullet NHCl + H_2O$	1.02×10^{9} $M^{-1}s^{-1}$	3
S27	$NH_2Cl + \bullet Cl \rightarrow \bullet NHCl + Cl^-$	1.00×10^{9} $M^{-1}s^{-1}$	3
S28	$NH_2Cl + \bullet Cl_2^- \rightarrow \bullet NHCl + 2Cl^- + H^+$	1.14×10^{7} $M^{-1}s^{-1}$	6,7
S29	$NHCl_2 + \bullet OH \rightarrow NCl_2\bullet + H_2O$	6.21×10^{8} $M^{-1}s^{-1}$	This study
S30	$NHCl_2 + \bullet Cl \rightarrow NCl_2\bullet + Cl^- + H^+$	1.00×10^{9} $M^{-1}s^{-1}$	Assumed
S31	$NHCl_2 + \bullet Cl_2^- \rightarrow NCl_2\bullet + 2Cl^- + H^+$	4.4×10^{6} $M^{-1}s^{-1}$	6
Reactions of $\bullet NH_2$ and NHCl•			
S32	$\bullet NH_2 + O_2 \rightarrow NH_2O_2\bullet$	1.2×10^{8} $M^{-1}s^{-1}$	8, 9
S33	$\bullet NHCl + O_2 \rightarrow NHClO_2\bullet$	1.2×10^{8} $M^{-1}s^{-1}$	10
S34	$NH_2O_2\bullet \rightarrow \bullet NO + H_2O$	1.0×10^{8} s^{-1}	Assumed
S35	$NHClO_2\bullet \rightarrow \bullet NO$ + product	1.0×10^{8} s^{-1}	Assumed
S36	$NH_2O_2\bullet \rightarrow$ transient species $\rightarrow N_2O$	5.98×10^{8} s^{-1}	Estimated
S37	$NHClO_2\bullet \rightarrow$ transient species $\rightarrow N_2O$	6.7×10^{8} s^{-1}	Estimated

S38	$\bullet NO + \bullet OH \rightarrow NO_2^- + H^+$	$1.0 \times 10^{10}\ M^{-1}s^{-1}$	11
S39	$NO_2^- + \bullet OH \rightarrow \bullet NO_2 + OH^-$	$1.2 \times 10^{10}\ M^{-1}s^{-1}$	12
S40	$\bullet NO + \bullet NO + O_2 \rightarrow 2\ \bullet NO_2$	$2.1 \times 10^{6}\ M^{-2}s^{-1}$	13
S41	$\bullet NO + \bullet NO_2 \rightarrow N_2O_3$	$1.1 \times 10^{9}\ M^{-1}s^{-1}$	13
S42	$N_2O_3 \rightarrow \bullet NO + \bullet NO_2$	$4.3 \times 10^{6}\ s^{-1}$	13
S43	$N_2O_3 + H_2O \rightarrow 2NO_2^- + 2H^+$	$1.6 \times 10^{3}\ s^{-1}$	13
S44	$\bullet NO_2 + \bullet NO_2 \rightarrow N_2O_4$	$4.5 \times 10^{8}\ M^{-1}s^{-1}$	14
S45	$N_2O_4 + H_2O \rightarrow NO_2^- + NO_3^- + 2H^+$	$1.0 \times 10^{3}\ s^{-1}$	14
Reactions with organic compounds			
S46	$\bullet OH + CH_3COO^- \rightarrow \bullet CH_2COO^- + H_2O$	$7.50\times10^{7}\ M^{-1}s^{-1}$	15
S47	$\bullet Cl + CH_3COO^- \rightarrow \bullet CH_2COO^- + HCl$	$3.70\times10^{9}\ M^{-1}s^{-1}$	16
S48	$\bullet OH + CH_3COOH \rightarrow \bullet CH_2COO^- + H_2O$	$1.50\times10^{7}\ M^{-1}s^{-1}$	17, 18
S49	$\bullet Cl + CH_3COOH \rightarrow \bullet CH_2COO^- + HCl$	$2.00\times10^{8}\ M^{-1}s^{-1}$	19
S50	$\bullet O^- + CH_3COO^- \rightarrow \bullet CH_2COO^- + OH^-$	$5.00\times10^{7}\ M^{-1}s^{-1}$	20
S51	1,4-dioxane + $\bullet OH \rightarrow$ product	$3.1\times10^{9}\ M^{-1}s^{-1}$	6
S52	1,4-dioxane + $\bullet Cl \rightarrow$ product	$4.4\times10^{6}\ M^{-1}s^{-1}$	6
S53	1,4-dioxane + $\bullet Cl_2^- \rightarrow$ product	$3.3\times10^{6}\ M^{-1}s^{-1}$	6
S54	DOC + $\bullet OH \rightarrow$ product	$3.3 \times10^{4}\ (mg/L)^{-1}s^{-1}$	21
Other reactions			
S55	$H_2O \rightarrow H^+ + OH^-$	$1.00\times10^{-3}\ s^{-1}$	2
S56	$H^+ + OH^- \rightarrow H_2O$	$1.00\times10^{11}\ M^{-1}s^{-1}$	2
S57	$H_2O_2 \rightarrow H^+ + HO_2^-$	$1.26\times10^{-1}\ s^{-1}$	2
S58	$H^+ + HO_2^- \rightarrow H_2O_2$	$5.00\times10^{10}\ M^{-1}s^{-1}$	2
S59	$\bullet OH + H_2O_2 \rightarrow HO_2\bullet + H_2O$	$2.70\times10^{7}\ M^{-1}s^{-1}$	22
S60	$\bullet OH + \bullet OH \rightarrow H_2O_2$	$5.50\times10^{9}\ M^{-1}s^{-1}$	22
S61	$HO_2\bullet + H_2O_2 \rightarrow O_2 + \bullet OH + H_2O$	$3.00\ M^{-1}s^{-1}$	23
S62	$O_2\bullet^- + H_2O_2 \rightarrow O_2 + \bullet OH + OH^-$	$1.30\times10^{-1}\ M^{-1}s^{-1}$	23
S63	$HO_2\bullet + HO_2\bullet \rightarrow O_2 + H_2O_2$	$8.30\times10^{5}\ M^{-1}s^{-1}$	23
S64	$HO_2\bullet + O_2\bullet^- \rightarrow O_2 + HO_2^-$	$9.70\times10^{7}\ M^{-1}s^{-1}$	23
S65	$\bullet OH + HO_2\bullet \rightarrow O_2 + H_2O$	$6.60\times10^{9}\ M^{-1}s^{-1}$	23

S66	$\bullet OH + O_2\bullet^- \rightarrow O_2 + OH^-$	7.00×10^{9} $M^{-1}s^{-1}$	[23]
S67	$\bullet OH + HO_2^- \rightarrow HO_2\bullet + OH^-$	7.50×10^{9} $M^{-1}s^{-1}$	[23]
S68	$\bullet OH + OH^- \rightarrow O\bullet^- + H_2O$	1.20×10^{10} $M^{-1}s^{-1}$	[24]
S69	$\bullet OH + Cl^- \rightarrow ClOH\bullet^-$	4.30×10^{9} $M^{-1}s^{-1}$	[25]
S70	$ClOH\bullet^- \rightarrow Cl^- + \bullet OH$	6.10×10^{9} s^{-1}	[25]
S71	$\bullet Cl + H_2O \rightarrow ClOH\bullet^- + H^+$	2.50×10^{5} s^{-1}	[26]
S72	$\bullet Cl + OH^- \rightarrow ClOH\bullet^-$	1.80×10^{10} $M^{-1}s^{-1}$	[27]
S73	$\bullet Cl + Cl^- \rightarrow Cl_2\bullet^-$	8.00×10^{9} $M^{-1}s^{-1}$	[28]
S74	$Cl_2\bullet^- \rightarrow \bullet Cl + Cl^-$	6.00×10^{4} s^{-1}	[29]
S75	$Cl_2\bullet^- + H_2O \rightarrow Cl^- + HClOH$	1.30×10^{3} s^{-1}	[26]
S76	$HClOH \rightarrow ClOH\bullet^- + H^+$	1.00×10^{8} s^{-1}	[26]
S77	$ClOH\bullet^- + Cl^- \rightarrow Cl_2\bullet^- + OH^-$	1.00×10^{4} $M^{-1}s^{-1}$	[30]
S78	$ClOH\bullet^- + H^+ \rightarrow \bullet Cl + H_2O$	2.10×10^{10} $M^{-1}s^{-1}$	[25]
S79	$\bullet Cl + H_2O_2 \rightarrow HO_2\bullet + Cl^- + H^+$	2.00×10^{9} $M^{-1}s^{-1}$	[29]
S80	$\bullet Cl + \bullet Cl \rightarrow Cl_2$	8.80×10^{7} $M^{-1}s^{-1}$	[31]
S81	$Cl_2\bullet^- + \bullet OH \rightarrow HOCl + Cl^-$	1.00×10^{9} $M^{-1}s^{-1}$	[32]
S82	$Cl_2\bullet^- + Cl_2\bullet^- \rightarrow Cl_2 + 2Cl^-$	9.00×10^{8} $M^{-1}s^{-1}$	[29]
S83	$Cl_2\bullet^- + \bullet Cl \rightarrow Cl_2 + Cl^-$	2.10×10^{9} $M^{-1}s^{-1}$	[29]
S84	$Cl_2\bullet^- + H_2O_2 \rightarrow HO_2\bullet + 2Cl^- + H^+$	1.40×10^{5} $M^{-1}s^{-1}$	[33]
S85	$Cl_2\bullet^- + HO_2\bullet \rightarrow 2Cl^- + H^+ + O_2$	3.00×10^{9} $M^{-1}s^{-1}$	[33]
S86	$Cl_2\bullet^- + O_2\bullet^- \rightarrow 2Cl^- + O_2$	2.00×10^{9} $M^{-1}s^{-1}$	[33]
S87	$Cl_2\bullet^- + OH^- \rightarrow ClOH\bullet^- + Cl^-$	4.50×10^{7} $M^{-1}s^{-1}$	[30]
S88	$Cl_3^- \rightarrow Cl_2 + Cl^-$	1.10×10^{5} s^{-1}	[34]
S89	$Cl_3^- + HO_2\bullet \rightarrow Cl_2\bullet^- + HCl + O_2$	1.00×10^{9} $M^{-1}s^{-1}$	[35]
S90	$Cl_3^- + O_2\bullet^- \rightarrow Cl_2\bullet^- + Cl^- + O_2$	3.80×10^{9} $M^{-1}s^{-1}$	[33]
S91	$Cl_2 + H_2O \rightarrow HOCl + Cl^- + H^+$	15 s^{-1}	[36]
S92	$Cl_2 + Cl^- \rightarrow Cl_3^-$	2.00×10^{4} $M^{-1}s^{-1}$	[34]
S93	$Cl_2 + H_2O_2 \rightarrow 2HCl + O_2$	1.30×10^{4} $M^{-1}s^{-1}$	[33]
S94	$Cl_2 + O_2\bullet^- \rightarrow Cl_2\bullet^- + O_2$	1.00×10^{9} $M^{-1}s^{-1}$	[33]
S95	$Cl_2 + HO_2\bullet \rightarrow Cl_2\bullet^- + H^+ + O_2$	1.00×10^{9} $M^{-1}s^{-1}$	[35]

S96	$HOCl \rightarrow OCl^- + H^+$	1.41×10^3 s^{-1}	2
S97	$OCl^- + H^+ \rightarrow HOCl$	5.00×10^{10} $M^{-1}s^{-1}$	2
S98	$HOCl + H_2O_2 \rightarrow HCl + H_2O + O_2$	1.10×10^4 $M^{-1}s^{-1}$	37
S99	$OCl^- + H_2O_2 \rightarrow Cl^- + H_2O + O_2$	1.70×10^5 $M^{-1}s^{-1}$	37
S100	$HOCl + O_2{\bullet}^- \rightarrow {\bullet}Cl + OH^- + O_2$	7.50×10^6 $M^{-1}s^{-1}$	38
S101	$HOCl + HO_2{\bullet} \rightarrow {\bullet}Cl + OH^- + O_2$	7.50×10^6 $M^{-1}s^{-1}$	33
S102	$OCl^- + O_2{\bullet}^- + H_2O \rightarrow {\bullet}Cl + 2OH^- + O_2$	2.00×10^8 $M^{-2}s^{-1}$	33
S103	$H^+ + Cl^- \rightarrow HCl$	5.00×10^{10} $M^{-1}s^{-1}$	2
S104	$HCl \rightarrow H^+ + Cl^-$	8.60×10^{16} s^{-1}	2
S105	$H^+ + NH_2Cl + NO_2^- \xrightarrow{\text{Rate-limiting}} NH_3 + NO_2Cl \rightarrow NO_3^-$	1.36×10^7 $M^{-2}s^{-1}$	39
S106	${\bullet}OH + HPO_4^{2-} \rightarrow HPO_4{\bullet}^- + OH^-$	1.50×10^5 $M^{-1}s^{-1}$	23
S107	${\bullet}OH + H_2PO_4^- \rightarrow HPO_4{\bullet}^- + H_2O$	2.00×10^4 $M^{-1}s^{-1}$	23
S108	$H_2O_2 + HPO_4{\bullet}^- \rightarrow H_2PO_4^- + HO_2{\bullet}$	2.70×10^7 $M^{-1}s^{-1}$	23
S109	${\bullet}OH + HCO_3^- \rightarrow CO_3{\bullet}^- + H_2O$	8.50×10^6 $M^{-1}s^{-1}$	23
S110	${\bullet}OH + H_2CO_3 \rightarrow CO_3{\bullet}^- + H_2O + H^+$	1.00×10^6 $M^{-1}s^{-1}$	3
S111	${\bullet}OH + CO_3{\bullet}^- \rightarrow$ product	3.00×10^9 $M^{-1}s^{-1}$	23
S112	$H_2O_2 + CO_3{\bullet}^- \rightarrow HCO_3^- + HO_2{\bullet}$	4.30×10^5 $M^{-1}s^{-1}$	23
S113	$HO_2^- + CO_3{\bullet}^- \rightarrow CO_3^{2-} + HO_2{\bullet}$	3.00×10^7 $M^{-1}s^{-1}$	23
S114	$O_2{\bullet}^- + CO_3{\bullet}^- \rightarrow CO_3^{2-} + O_2$	6.00×10^8 $M^{-1}s^{-1}$	23
S115	$CO_3{\bullet}^- + CO_3{\bullet}^- \rightarrow$ product	3.00×10^7 $M^{-1}s^{-1}$	23

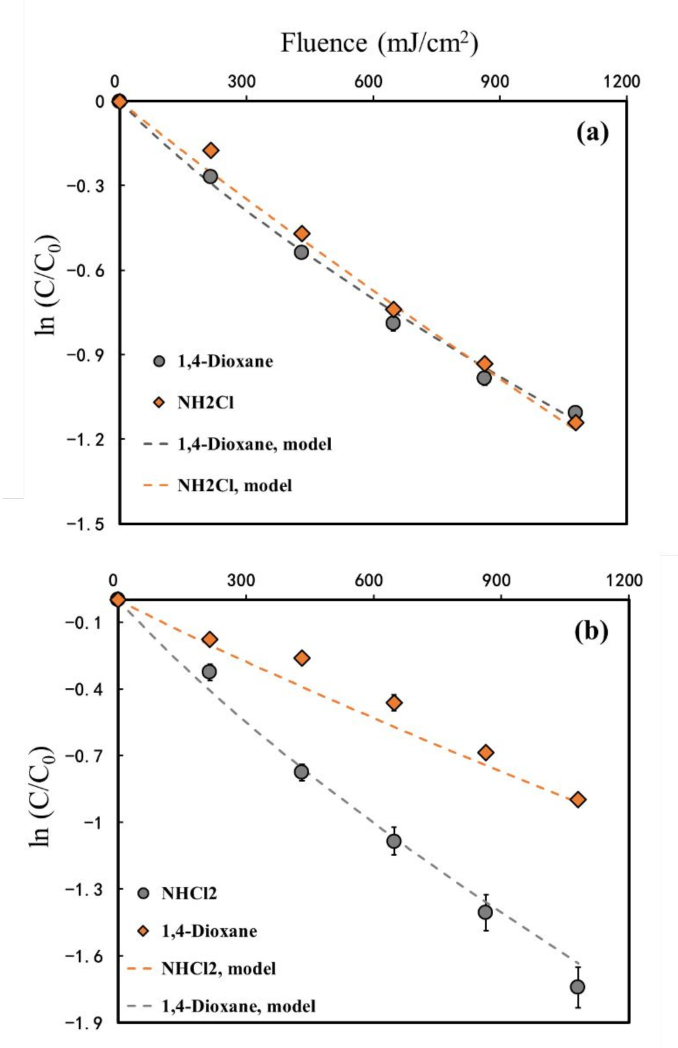

Figure S1. Plots of $\ln(C/C_0)$ vs. t for the (a) UV/NH_2Cl (47 µM) AOP and the (b) UV/$NHCl_2$ (44 µM) AOP treating 0.2 µM 1,4-dioxane. The modeled results were determined using the optimized model from the manuscript (Table S3).

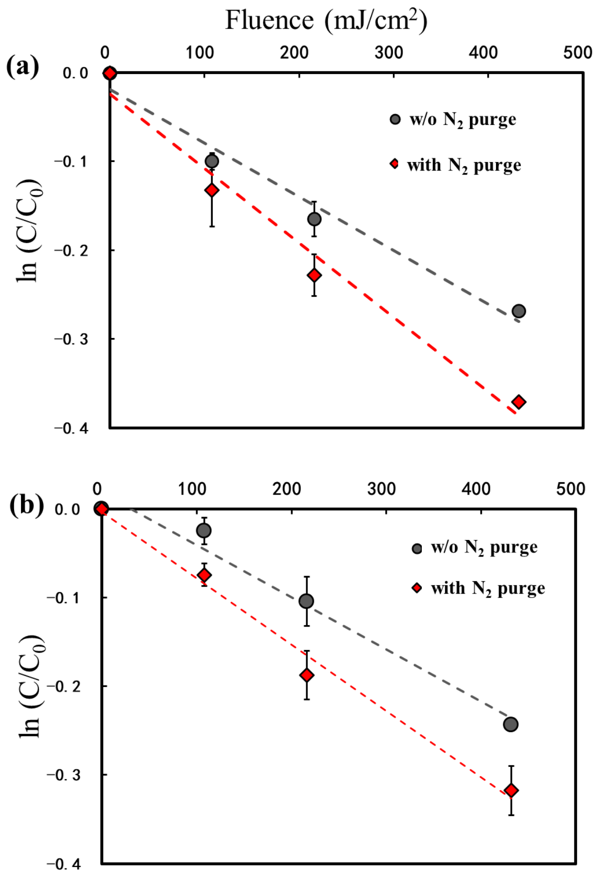

Figure S2. Photodecomposition of (a) NH_2Cl (50 μM) and (b) $NHCl_2$ (50 μM) in 2 mM phosphate buffer with N_2 purge and without N_2 purge. Error bars represent the data range of experimental duplicates.

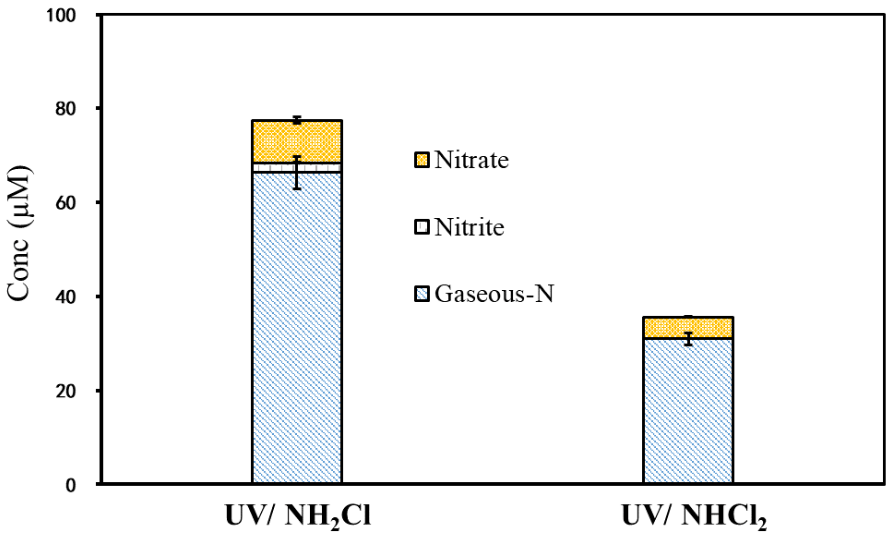

Figure S3. Formation of nitrite and nitrate and gaseous nitrogen loss from chloramine (100 µM) photolysis in 2 mM phosphate buffer. Error bars represent the data range of experimental duplicates.

Text S3. Procedure to determine the innate quantum yields of chloramines by modeling

The quantum yields of NH_2Cl and $NHCl_2$ were determined by experimental data for oxidant decay from experiments using different initial concentrations of NH_2Cl and $NHCl_2$, both with and without acetate as a radical quenching agent, using a kinetics model combining the 94 elementary reactions listed in Table S3. The procedure was described in our previous study.[3] The optimal innate Φ for oxidants was determined using least squares fitting, where the sum of the squares of errors (SSE) is defined as: $SSE = \sum(k_{modeled} - k_{obs})^2$; k_{obs} represents the experimentally determined (pseudo-first order) rate constants for oxidant decay. Table S4 shows the k_{obs} for oxidant decay, the modeled k for oxidant decay using various Φ, and the corresponding SSE. Figure S4 shows the optimal quantum yields with the smallest SSE.

Table S4. k_{obs} for oxidant decay, the modeled k for oxidant decay using various Φ, and the sum of squares of errors.

Experiments			Modeled k (cm^2/mJ)					
$[NH_2Cl]_{initial}$ (μM)	[Acetate] (μM)	k_{obs} (cm^2/mJ)	Φ = 0.10	Φ = 0.20	Φ = 0.30	Φ = 0.35	Φ = 0.40	Φ = 0.50
10	0	0.00111	0.00035	0.00066	0.00095	0.00109	0.00122	0.00148
20	0	0.00109	0.00035	0.00068	0.00099	0.00113	0.00127	0.00154
50	0	0.00109	0.00036	0.00071	0.00105	0.00120	0.00136	0.00166
10	500	0.00087	0.00035	0.00066	0.00095	0.00067	0.00122	0.00096
20	1000	0.00080	0.00019	0.00038	0.00058	0.00067	0.00077	0.00096
50	2500	0.00093	0.00019	0.00039	0.00058	0.00068	0.00078	0.00098
$\Sigma(k_{modeled} - k_{obs})^2$			2.9×10^{-6}	1.0×10^{-6}	2.2×10^{-7}	1.3×10^{-7}	2.7×10^{-7}	7.0×10^{-7}

Experiments			Modeled k (cm^2/mJ)					
$[NHCl]_{]initial}$ (μM)	[Acetate] (μM)	k_{obs} (cm^2/mJ)	Φ = 0.60	Φ = 0.70	Φ = 0.72	Φ = 0.75	Φ = 0.80	Φ = 0.90
4	0	0.00065	0.00067	0.00077	0.00079	0.00082	0.00086	0.00087
10	0	0.00082	0.00068	0.00078	0.00080	0.00083	0.00088	0.00099
25	0	0.00081	0.00068	0.00079	0.00081	0.00084	0.00089	0.00099
50	0	0.00076	0.00069	0.00079	0.00081	0.00084	0.00089	0.00099
4	200	0.00058	0.00042	0.00049	0.00050	0.00052	0.00056	0.00063
10	500	0.00071	0.00041	0.00048	0.00049	0.00051	0.00054	0.00061
25	1250	0.00066	0.00040	0.00047	0.00048	0.00050	0.00054	0.00060
50	2500	0.00056	0.00040	0.00047	0.00048	0.00050	0.00053	0.00060
	$\Sigma(k_{modeled} - k_{obs})^2$		2.47×10^{-7}	1.23×10^{-7}	1.13×10^{-7}	1.07×10^{-7}	1.17×10^{-7}	1.76×10^{-7}

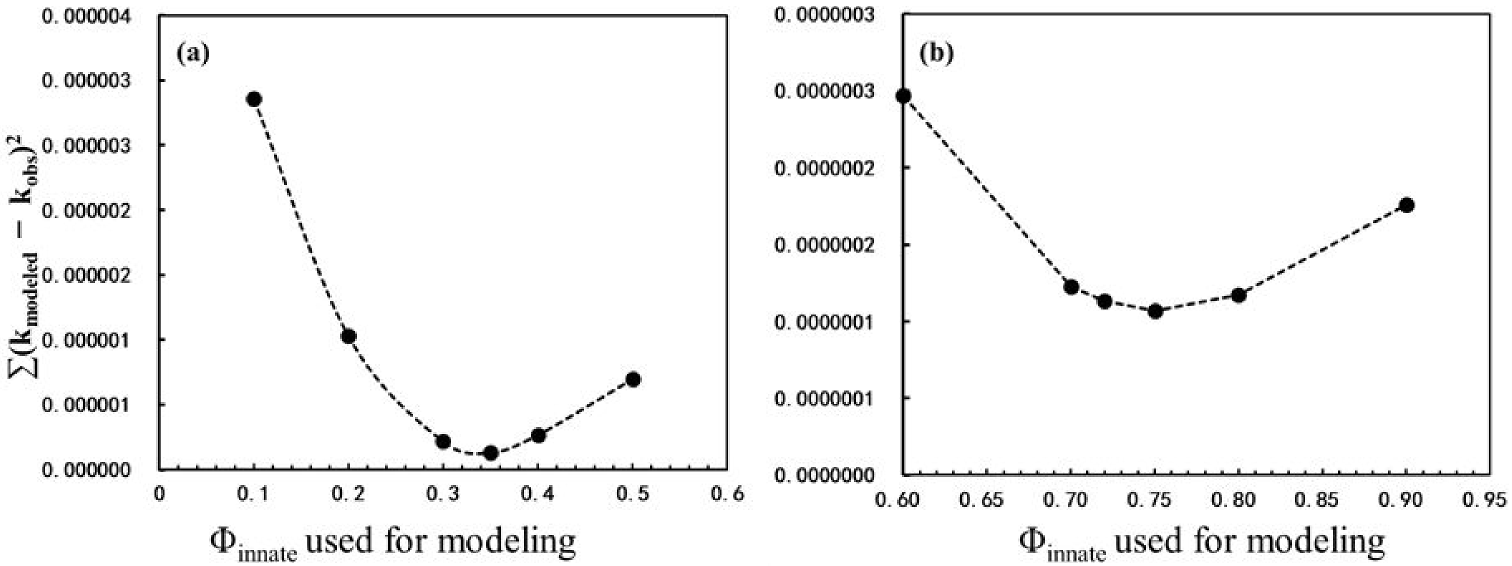

Figure S4. Sum of the squares of errors for predicted vs. measured loss of oxidants using data from all experiments (i.e., with and without acetate) and using various Φ for (a) NH_2Cl and (b) $NHCl_2$.

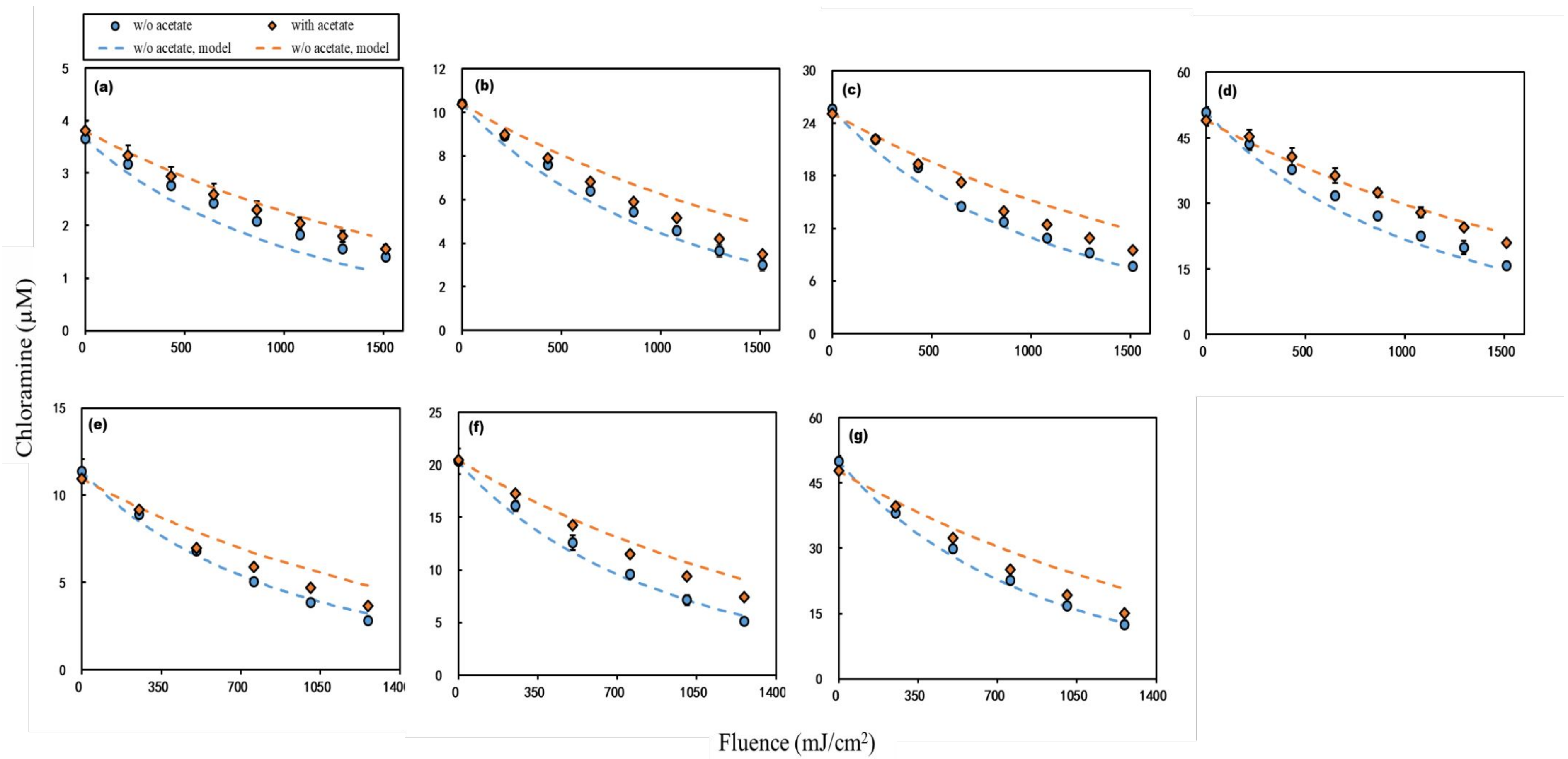

Figure S5. Experimental vs modeled results of photolysis of $NHCl_2$ (a-d) and NH_2Cl (e-g) over a range of chloramine concentrations (4 – 50 μM) with and without the quencher. Error bars represent the data range of experimental duplicates.

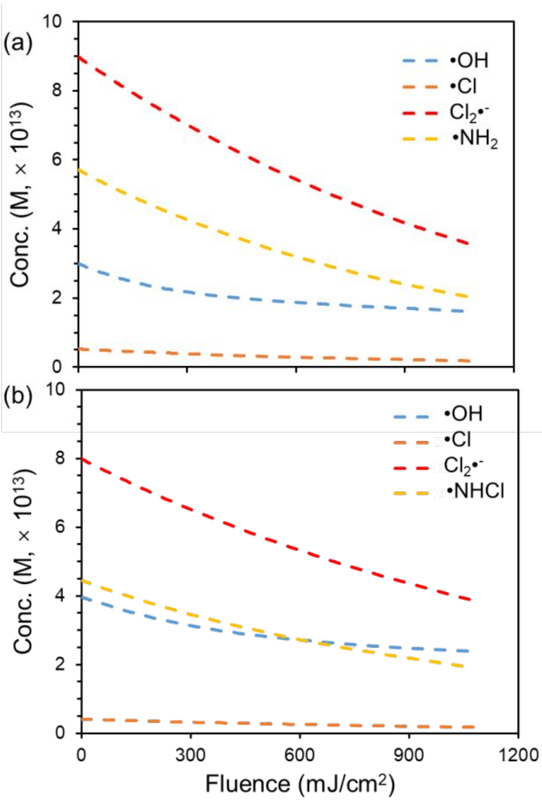

Figure S6. Variation of modeled radical concentrations during (a) UV/NH_2Cl (46 μM) AOP and (b) UV/$NHCl_2$ (45 μM) AOP treatment of 0.2 μM 1,4-dioxane in 2 mM phosphate buffer.

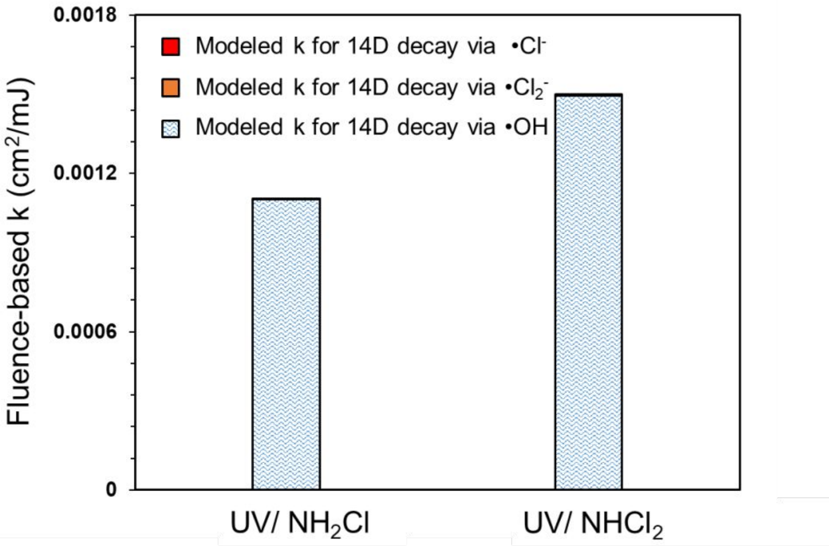

Figure S7. Modeled fluence-based k for 1,4-dioxane decay via $^{\bullet}OH$, $Cl^{\bullet -}$ and $Cl_2^{\bullet -}$ during the UV/NH_2Cl (46 µM) and the UV/$NHCl_2$ (45 µM) AOP treatment of 0.2 µM 1,4-dioxane.

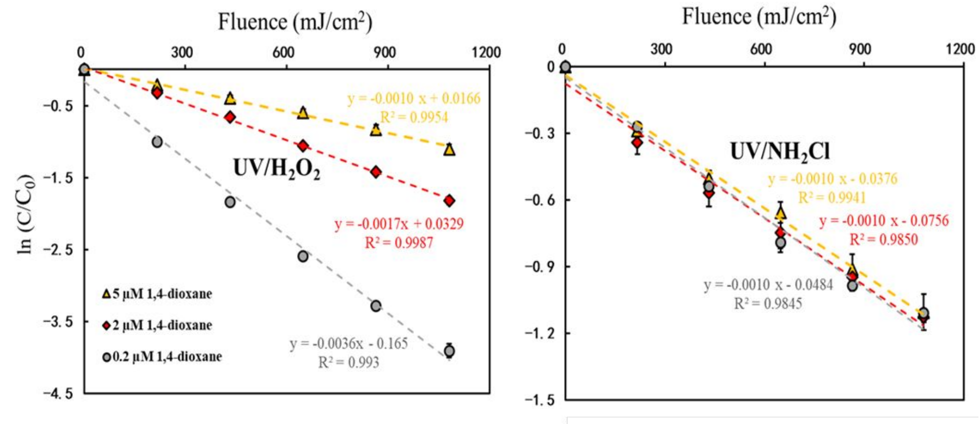

Figure S8: Effect of 1,4-dioxane concentration (0.2-5 μM) on its pseudo-first-order degradation rate for UV/H_2O_2 (100 μM H_2O_2) and UV/NH_2Cl (50 μM NH_2Cl) in 2 mM phosphate at pH 5.5. Error bars represent the data range of experimental duplicates.

Text S4: Determining $k_{\bullet OH}$ for $NHCl_2$ and dissolved organic carbon in the RO permeate using gamma-radiolysis

The hydroxyl radical reaction rate constant for $NHCl_2$ was determined by gamma radiolysis as described in our previous study.[5] Deionized water (500 mL) buffered with 5 mM phosphate was adjusted to pH 5.0 with phosphoric acid and purged with N_2O gas for >40 minutes. The sample was spiked with 15 μM $NHCl_2$ and 1 μM tribromomethane (TBM, reference compound), and then decanted into 25-mL vials. The vials were sealed headspace-free with Teflon-lined septa. Samples were exposed to gamma radiation within a Mark I Model 25 irradiator (JL Shepherd and Associates, San Fernando, CA, USA) employing a ^{137}Cs source.

The $^{\bullet}OH$ reaction rate constants were determined by competition kinetics, using bromoform (k_{OH} = 1.5×10^8 M^{-1} s^{-1})[40] as the reference compound. Two earlier studies have indicated reaction rate constants of 1.3×10^8 M^{-1} s^{-1} [41] and 1.1×10^8 M^{-1} s^{-1} [42]. Samples periodically removed from the device were sacrificed and analyzed for the residual target compound (T) and the reference compound (R). Using the $^{\bullet}OH$ reaction rate constants with the reference compounds (k_R), the $^{\bullet}OH$ reaction rate constant with the target compound (k_T) was determined from the slope of plots of $\ln([T]/[T]_0)$ vs. $\ln([R]/[R]_0)$ according to:[43]

$$\ln\left(\frac{[T]}{[T]_0}\right) = \frac{k_T}{k_R}\ln\left(\frac{[R]}{[R]_0}\right)$$

Figure S9 shows the results. Accordingly, we obtained the •OH rate constant with $NHCl_2$ to be $6.21\ (\pm 0.07) \times 10^8$ M^{-1} s^{-1} (average ± range of experimental duplicates).

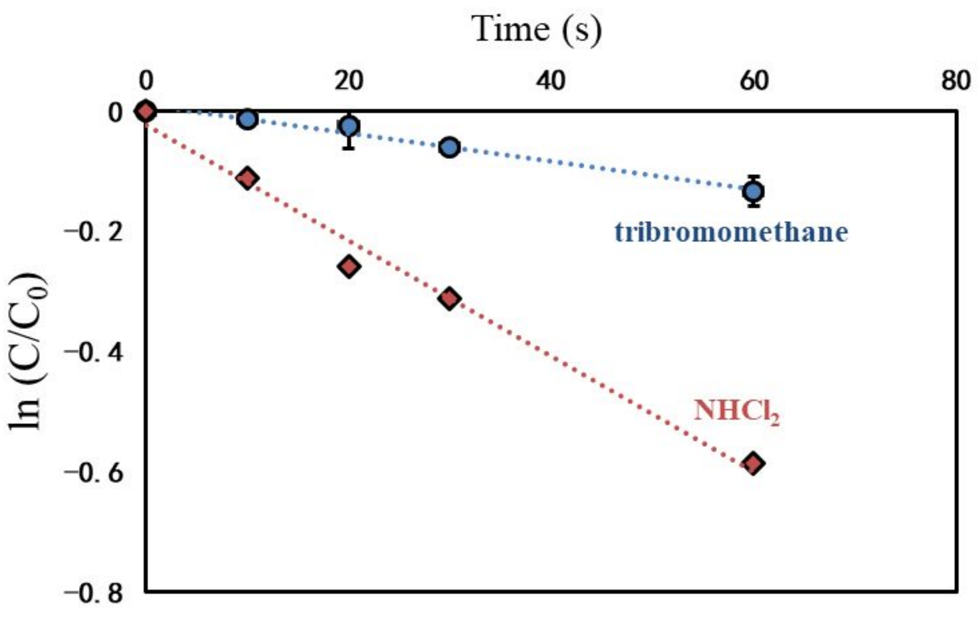

Figure S9. Gamma-radiolysis experiments for determining $k_{\bullet OH}$ for $NHCl_2$.

We also used competition kinetics to determine the •OH reaction rate constant with the DOC in RO permeate. Two samples of RO permeate were collected from Facility 1 during two separate sampling events. The residual chloramines were measured by the DPD colorimetric method and then quenched using stoichiometric sodium sulfite. The DOC concentrations were 0.21 mg-C/L and 0.33 mg-C/L for sample 1 and sample 2, respectively (Table S1). Dissolved inorganic carbon was measured using a Shimadzu TOC-L analyzer. The total inorganic carbon (i.e., carbonate) concentrations were 0.15 mM, which were lower than the concentrations (0.5 mM) measured on the sampling days due to off-gassing of CO_2 into the headspace of the storage bottles. The samples were buffered with 5 mM phosphate at pH 5.0 and purged with N_2O gas for > 40 mins. Purging with N_2O was expected to further reduce the carbonate concentration. The samples were then spiked with 1 μM tribromomethane and decanted into 25-mL vials. The vials were sealed headspace-free with Teflon-lined septa, and treated by gamma radiolysis, as described above. The losses of tribromomethane in the RO permeate samples were compared to the loss in deionized water spiked with 15 μM $NHCl_2$, as shown in Figure S10. The slopes of $\ln(C/C_0)$ vs t provided the pseudo-first order degradation rate constants (k_{obs}) for tribromomethane. The k_{obs} was determined by the steady-state concentration of •OH ($[\bullet OH]_{ss}$) as shown in equation S116:

$$-\frac{d[TBM]}{dt} = k_{obs}[TBM] = k_{\bullet OH,TBM}[\bullet OH]_{ss}[TBM] \quad \text{(S116)}$$

where k_{obs} is the pseudo-first order degradation rate constant for TBM (s^{-1}), $k_{\bullet OH,TBM}$ is the second order •OH reaction rate constant with TBM ($M^{-1}\ s^{-1}$). $[\bullet OH]_{ss}$ can be calculated by the ratio of the •OH production rate to the •OH scavenging rate ($[\bullet OH]_{ss} = \frac{\text{Production rate}}{\text{Scavenging rate}}$). In deionized water, $NHCl_2$ dominated •OH scavenging as shown in Table S5. Accordingly, $[\bullet OH]_{ss}$ in this system can be described by equation S117:

$$[\bullet OH]_{ss,\,DI} = \frac{\text{Production rate}}{\text{Scavenging rate}} \cong \frac{Production\ rate}{k_{\bullet OH,NHCl2} \times [NHCl2]} \quad \text{(S117)}$$

where $[\bullet OH]_{ss,DI}$ represents the steady-state concentration of •OH in deionized (DI) water spiked with 1 μM TBM and 15 μM $NHCl_2$, $k_{\bullet OH,NHCl2}$ is the second order •OH reaction rate constant with $NHCl_2$ ($M^{-1}\ s^{-1}$), and $[NHCl_2]$ is the concentration of $NHCl_2$ (M).

In RO permeate spiked only with TBM, TBM degradation was somewhat faster than in deionized water spiked with both TBM and $NHCl_2$, but by less than a factor of two (Figure S10). The similarity suggests a similar $[\bullet OH]_{ss}$, and that the overall •OH scavenging must be at least half that of 15 μM $NHCl_2$. Considering the relatively low contribution to •OH scavenging from TBM and other inorganic species in the system (Table S5), the DOC in RO permeate would be the dominant •OH scavenger. Thus, $[\bullet OH]_{ss}$ in RO permeate can be described by equation S118:

$$[\bullet OH]_{ss,\,RO} = \frac{\text{Production rate}}{\text{Scavenging rate}} \cong \frac{Production\ rate}{k_{\bullet OH,DOC} \times [DOC]} \quad \text{(S118)}$$

where $[\bullet OH]_{ss,\,RO}$ represents the steady-state concentration of •OH in RO permeate spiked with 1 μM TBM, $k_{\bullet OH,\,DOC}$ is the •OH rate constant with DOC $(mg\text{-}C/L)^{-1}\ s^{-1}$ and [DOC] is the concentration of

DOC in RO permeate (mg-C/L). Since the •OH production rate from treatment of water by gamma radiolysis would be the same in the deionized water or RO permeate experiments,[22] the •OH reaction rate constant with the DOC in RO permeate can be estimated by equation S119 (i.e., by dividing equation S117 by equation S118):

$$\frac{k_{obs,DI}}{k_{obs,RO}} = \frac{[\bullet OH]_{ss,DI}}{[\bullet OH]_{ss,RO}} = \frac{k_{\bullet OH,DOC} \times [DOC]}{k_{\bullet OH,NHCl2} \times [NHCl2]} \qquad (S119)$$

Accordingly, the $k_{\bullet OH,DOC}$ was estimated to be 2.49 (±0.11)×10^4 (mg-C/L)$^{-1}$ s^{-1} (average ± range of experimental duplicates) for sample 1 and 2.12 (±0.009)×10^4 (mg-C/L)$^{-1}$ s^{-1} for sample 2. To check the assumption that DOC would be the dominant •OH scavenger, the •OH scavenging rate by DOC for sample 2 would be 6996 s^{-1}, which is much higher than the other inorganic constituents (Table S5; note that chloramines were not present in the RO permeate samples since they had been quenched by sulfite).

Table S5. •OH scavenging rate for different species.

	Initial conc (μM)	$k_{\bullet OH}$ ($M^{-1}s^{-1}$)	•OH scavenging rate (s^{-1}) = $k_{\bullet OH}$ × conc
$NHCl_2$	15	6.2 × 10^8	9300
TBM	1	1.5 × 10^8	150
HPO_4^{2-}	31.3	1.5 × 10^5	4.7
$H_2PO_4^-$	4962	2.0 × 10^4	99
HCO_3^-	7.2	8.5 × 10^6	61
H_2CO_3	143	1.0 × 10^6	143

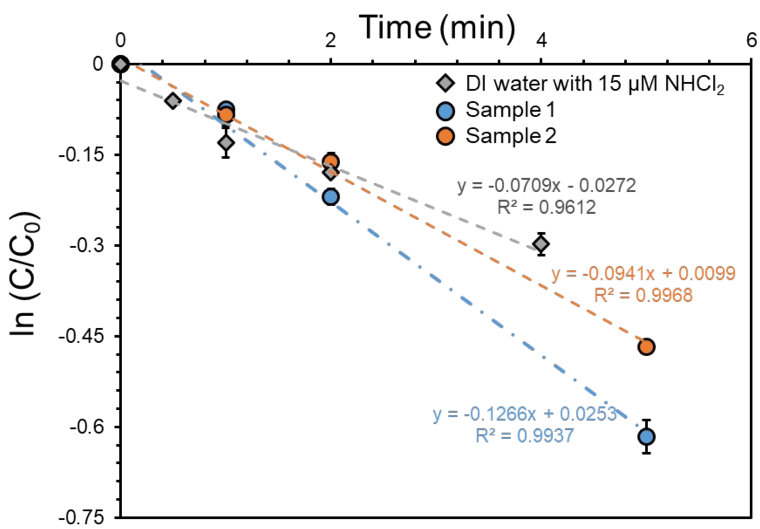

Figure S10. Degradation of tribromomethane in deionized water with 15 μM $NHCl_2$ and in the RO permeate samples collected from Facility 1.

Calculation of the contribution of different scavengers for reacting with radicals: In Figure 4, the total radicals produced for each AOP were distinguished by their fates. The cumulative radicals scavenged by different species, including carbonate, 1,4-dioxane (14D), $^{\bullet}$NO, oxidants and DOC, after 1080 mJ/cm^2 fluence were calculated by Kintecus 4.55 based on the equations below:

Total radical production (M) = $\int 2.303(\Phi_{NH2Cl}\varepsilon_{NH2Cl}I_0[NH_2Cl] + \Phi_{NHCl2}\varepsilon_{NHCl2}I_0[NHCl_2] + \Phi_{H2O2}\varepsilon_{H2O2}I_0[H_2O_2])dt$

(S120)

Radical scavenged by carbonate (M) = $\int (k_{HCO3-,\ \bullet OH}[^{\bullet}OH][HCO_3^-] + k_{H2CO3,\ \bullet OH}[^{\bullet}OH][H_2CO_3])\ dt$

(S121)

Radical scavenged by 14D (M) = $\int [(k_{14D,\ \bullet OH}[^{\bullet}OH] + k_{14D,\ \bullet Cl}[^{\bullet}Cl] + k_{14D,Cl2\bullet -}[Cl_2^{\bullet -}])[14D]]dt$

(S122)

Radical scavenged by $^{\bullet}$NO (M) = $\int (k_{\bullet NO,\ \bullet OH}[^{\bullet}OH][^{\bullet}NO] + k_{NO2^-,\ \bullet OH}[^{\bullet}OH][NO_2^-])dt$

(S123)

Radical scavenged by oxidants (M) = $\int (k_{NH2Cl,\ \bullet OH}[^{\bullet}OH][NH_2Cl] + k_{NH2Cl,\ \bullet Cl}[^{\bullet}Cl][NH_2Cl] + k_{NH2Cl,\ Cl2^{\bullet -}}[Cl_2^{\bullet -}][NH_2Cl] + k_{NHCl2,\ \bullet OH}[^{\bullet}OH][NHCl_2] + k_{NHCl2,\ \bullet Cl}[^{\bullet}Cl][NHCl_2] + k_{NHCl2,\ Cl2^{\bullet -}}[Cl_2^{\bullet -}][NHCl_2] + k_{H2O2,\ \bullet OH}[^{\bullet}OH][H_2O_2] + k_{H2O2,\ \bullet Cl}[^{\bullet}Cl][H_2O_2] + k_{H2O2,\ Cl2^{\bullet -}}[Cl_2^{\bullet -}][H_2O_2])dt$ (S124)

Radical scavenged by DOC (M) = $\int k_{DOC,\ \bullet OH}[^{\bullet}OH][DOC]dt$

(S125)

where Φ is the photolysis quantum yield in mol/Einstein, ε is the molar absorption coefficient (M^{-1} cm^{-1}), I_0 is the incident light intensity (mEin cm^{-2} s^{-1}), and $k_{i,j}$ represents the rate constant between i and j (M^{-1}s^{-1}).

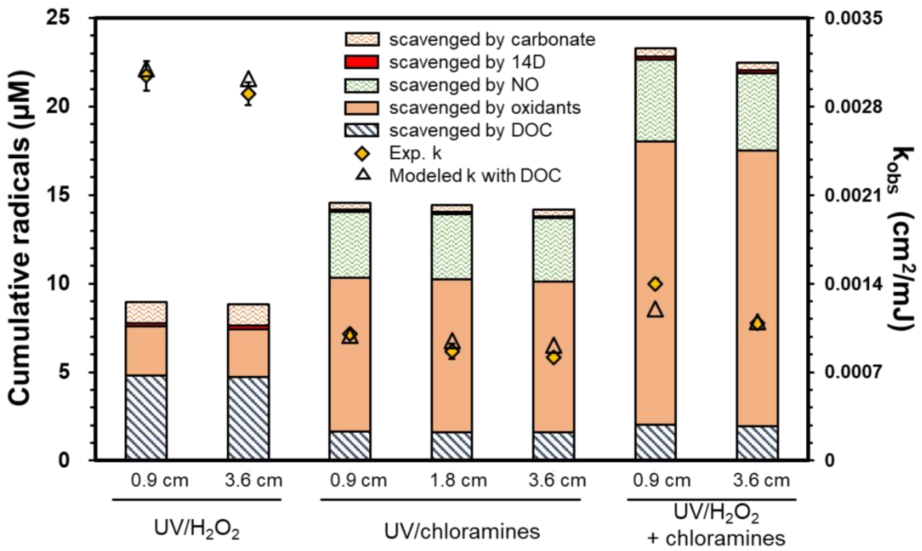

Figure S11. Experimental and modeled fluence-based pseudo-first order rate constants (k_{obs}) for loss of 0.2 μM 1,4-dioxane during various AOP treatments in authentic RO permeate (Facility 1 Event 1) with different light pathlengths. Using the model considering radical scavenging by DOC, the total radicals produced for each AOP after 1080 mJ/cm^2 fluence were distinguished by their fates.

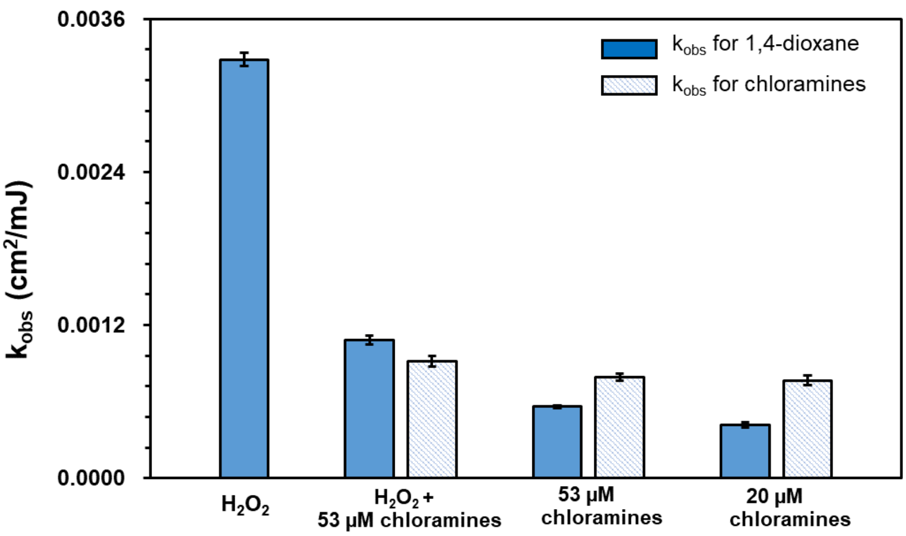

Figure S12. Pseudo-first order observed fluence-based rate constants for the degradation of 0.2 μM 1,4-dioxane and the chloramines in the RO permeate sample from Facility 2 for a light pathlength of 3.6 cm. The sample contained 35 μM NH_2Cl and 9 μM $NHCl_2$ (53 μM Cl[+1] chloramines). For the UV/H_2O_2 AOP, residual chloramines were quenched using stoichiometric sodium sulfite prior to adding 100 μM H_2O_2. For the UV/H_2O_2-chloramines AOP, 100 μM H_2O_2 was added to the background chloramines in the RO permeate. For the UV/chloramines AOP, either the background 53 μM chloramines were used or for 20 μM chloramines, sodium sulfite was added to partially quench the total residual chloramine concentration to 20 μM. Error bars represent the data range of experimental duplicates.

Text S5. Initial cost estimates for AOP alternatives

The cost estimates targeted 0.5-log removal of 1,4-dioxane, using a 3.6 cm light pathlength. The estimates considered as a baseline the UV/H_2O_2-chloramines AOP containing 50 µM total chloramines (3.3 mg/L as Cl_2) and 100 µM H_2O_2 (3.4 mg/L). The estimates also considered that the utility would attempt to reach a 35 µM (2.5 mg/L as Cl_2) chloramine residual for final distribution. For the UV/H_2O_2-chloramines baseline AOP, the pseudo-first order rate constant for 1,4-dioxane degradation with a 3.6 cm pathlength was 0.0011 mJ/cm^2 (Figure 5). Achieving 0.5-log removal of 1,4-dioxane would require ~1000 mJ/cm^2 UV fluence. After 1000 mJ/cm^2, the residual chloramine concentration would decrease to ~20 µM (Figure 3), while the residual H_2O_2 concentration would be ~90 µM with or without chloramines present (Figures 2, 3 and 5).

To evaluate the energy input required to achieve this target removal, other research[44] has indicated an energy requirement of ~0.3 kWh/kgal for 1-log removal of 1,4-dioxane in RO permeate using the UV/H_2O_2-chloramines AOP with 2 mg/L residual chloramines and 3 mg/L hydrogen peroxide. These concentrations are similar to those employed in the base case and were used for rough estimates of the energy consumption. Accordingly, for 0.5-log removal of 1,4-dioxane, we estimated that ~0.15 kWh/kgal of energy input would be needed for treatment by the UV/H_2O_2-chloramines AOP.

Alternative 1: Quenching residual chloramines with bisulfite before H_2O_2 addition and AOP treatment to convert to the UV/H_2O_2 AOP.

The k_{obs} for 1,4-dioxane degradation for the UV/H_2O_2 AOP with a 3.6 cm pathlength was 0.0032 cm^2/mJ (Figure S11), which was similar to the k_{obs} for a 0.9 cm pathlength (Figure 4) due to the low absorbance of 100 µM H_2O_2 (0.00186 cm^{-1}) and the lack of chloramines. Thus the UV fluence needed to degrade 0.5-log 1,4-dioxane could be reduced to 360 mJ/cm^2 by quenching chloramines prior to H_2O_2 addition. Thus only ~0.056 kWh/kgal of energy input would be needed for treatment by the UV/H_2O_2 AOP. For a \$0.16/kWh cost of electricity, the savings would be \$4.06/million liters (ML).

Quenching total residual chloramines using sodium bisulfite requires 1 mole equivalent of sodium bisulfite per mole of Cl[+1] chloramines. Assuming a cost for a 40% by weight solution of sodium bisulfite of \$1.57/gallon,[45] the cost for quenching 50 µM chloramines would be \$5.40/ML.

Chlorine must be added to leave the 35 µM (2.5 mg/L as Cl_2) chloramine residual for distribution. However, the 90 µM H_2O_2 residual would scavenge the chlorine, requiring 1 mole free chlorine per mole H_2O_2. With or without bisulfite quenching, the cost of chlorine addition to quench the 90 µM residual H_2O_2 would be the same.

However, the 20 μM chloramine residual following UV/H_2O_2-chloramines AOP treatment would contribute to the final chloramine residual for distribution, such that only 15 μM additional chloramines would be needed. The additional chloramines could be added using 15 μM sodium hypochlorite and ~18 μM ammonium sulfate, assuming a ~20% molar excess of ammonia added to form chloramines. With bisulfite quenching, the full 35 μM chloramines would need to be added, requiring 35 μM sodium hypochlorite and ~42 μM ammonium sulfate. Thus bisulfite addition would necessitate an additional 20 μM sodium hypochlorite and ~24 μM ammonium sulfate. Assuming a cost of $0.69/gallon for a 12.5% by weight solution of sodium hypochlorite,[46] the cost of free chlorine addition would be $2.16/ML. Assuming a cost of $2.70/gallon for a 40% by weight solution of ammonium sulfate,[47] the cost of ammonium sulfate addition would be $5.67/ML.

Overall, quenching the chloramine residual would save $4.06/ML in electricity costs, but increase chemical costs by a total of $13.22/ML, for a net increase in costs of $9.15/ML (Table S6). It is also important to note that it may not be possible to reduce the UV fluence to 360 mJ/cm^2, because higher UV fluence may be needed to achieve other water quality goals, such as the direct UV photolysis of NDMA. Thus, it may not be possible even to achieve the potential energy savings.

Alternative 2: Avoiding H_2O_2 addition to convert to the UV/chloramines AOP using the residual chloramines.

For ~50 μM background chloramine concentration in RO permeate, the k_{obs} for 1,4-dioxane degradation by the UV/H_2O_2-chloramines AOP was 0.0011 cm^2/mJ for a 3.6 cm pathlength for samples collected from both facilities (Figures 5 and S11), such that ~1000 mJ/cm^2 would be required to achieve 0.5-log removal. For the UV/chloramines AOP, the k_{obs} value was 0.00082 cm^2/mJ at the first facility (Figure 5) and 0.00056 cm^2/mJ at Facility 2 (Figure S11). The UV fluence required to achieve 0.5-log removal of 1,4-dioxane at Facility 1 would be ~1400 mJ/cm^2, while it would be ~2050 mJ/cm^2 at Facility 2. This would increase the electricity cost by $2.54/ML at Facility 1 and $6.67/ML at Facility 2. At Facility 2, additional fluence might be needed to achieve 0.5-log removal since the k_{obs} value decreased from 0.00056 cm^2/mJ for 50 μM chloramines to 0.00042 cm^2/mJ for 20 μM chloramines (Figure S11). The extent of this increase is difficult to predict without pilot-testing, but should be <25%.

Using the 0.0072 cm^2/mJ k_{obs} for chloramine degradation (Figures 5 and S11), the residual chloramines would be 18 μM at Facility 1, which is not significantly different from the 20 μM residual for the UV/H_2O_2-chloramines AOP base case. However, the 11 μM residual at Facility 2 would be significantly lower, necessitating additional sodium hypochlorite (9 μM or $0.97/ML) and ammonium hydroxide (11 μM or \$2.59/ML) to replace the chloramines lost due to the additional UV fluence.

The cost of hydrogen peroxide addition would be saved. Assuming \$2.75/gallon for a 50% by weight hydrogen peroxide stock solution,[48] the cost savings would be \$4.95/ML.

The cost of sodium hypochlorite addition to quench the 90 μM residual H_2O_2 would be avoided, saving \$9.73/ML.

Overall, if the RO permeate already contained 50 μM residual chloramines, avoiding H_2O_2 addition at Facility 1 would cost \$2.54/ML in additional electricity costs, but save \$14.68/ML in chemical costs, resulting in a net savings of \$12.13/ML (Table S5). At Facility 2, the additional electricity cost would be \$6.67/ML and the additional chemical cost to replace the chloramines lost due to the extra fluence would be \$3.56/ML, but the savings would again be \$14.68/ML for a net savings of \$4.44/ML (Table S5).

However, if the RO permeate contained only 20 μM residual chloramines, there would be an additional cost to boost the chloramine residual to 50 μM upstream of the AOP. If the RO permeate featured only 20 μM residual chloramines, 30 μM sodium hypochlorite and ~36 μM ammonium sulfate would need to be added upstream of the AOP to bring the chloramine concentration to 50 μM. The cost of sodium hypochlorite addition would be \$3.24/ML. The cost of ammonium sulfate would be \$8.49/ML. The total additional cost would be \$11.73/ML. In this case, the net savings for Facility 1 would be \$0.41/ML, but there would be a net cost for Facility 2 of \$7.29/ML (Table S5).

Table S6. Net cost estimate summary

Alternative 1		$/ML
Energy savings	$	(4.06)
Bisulfite cost	$	5.40
Hypochlorite cost	$	2.16
Ammonium sulfate cost	$	5.66
Net cost	**$**	**9.15**
Alternative 2 - 50 µM chloramines in RO permeate		
<u>Facility 1</u>		
Energy cost	$	2.54
Hydrogen peroxide savings	$	(4.95)
Hypochlorite to quench peroxide savings	$	(9.73)
Net cost	**$**	**(12.13)**
<u>Facility 2</u>		
Energy cost	$	6.67
Hypochlorite cost to replace lost chloramines	$	0.97
Ammonium sulfate cost to replace lost chloramines	$	2.59
Hydrogen peroxide savings	$	(4.95)
Hypochlorite to quench peroxide savings	$	(9.73)
Net cost	**$**	**(4.44)**
Alternative 2 - 20 µM chloramines in RO permeate		
<u>Facility 1</u>		
Energy cost	$	2.54
Hydrogen peroxide savings	$	(4.95)
Hypochlorite to quench peroxide savings	$	(9.73)
Hypochlorite to raise chloramines to 50 µM	$	3.24
Ammonium sulfate cost to raise chloramines to 50 µM	$	8.49
Net cost	**$**	**(0.41)**
<u>Facility 2</u>		
Energy cost	$	6.67
Hypochlorite cost	$	0.97
Ammonium sulfate cost	$	2.59
Hydrogen peroxide savings	$	(4.95)
Hypochlorite to quench peroxide savings	$	(9.73)
Hypochlorite to raise chloramines to 50 µM	$	3.24
Ammonium sulfate cost to raise chloramines to 50 µM	$	8.49
Net cost	**$**	**7.29**

References

1. Grebel, J. E.; Pignatello, J. J.; Mitch, W. A., Effect of halide ions and carbonates on organic contaminant degradation by hydroxyl radical-based advanced oxidation processes in saline waters. *Environ. Sci. Technol.* **2010,** *44*, (17), 6822-6828.

2. Yang, Y.; Pignatello, J. J.; Ma, J.; Mitch, W. A., Comparison of Halide Impacts on the Efficiency of Contaminant Degradation by Sulfate and Hydroxyl Radical-Based Advanced Oxidation Processes (AOPs). *Environ. Sci. Technol.* **2014,** *48*, (4), 2344-2351.

3. Chuang, Y. H.; Chen, S.; Chinn, C. J.; Mitch, W. A., Comparing the UV/Monochloramine and UV/Free Chlorine Advanced Oxidation Processes (AOPs) to the UV/Hydrogen Peroxide AOP Under Scenarios Relevant to Potable Reuse. *Environ Sci Technol* **2017,** *51*, (23), 13859-13868.

4. Ianni, J. C. *Kintecus , Windows Version 4.55. www.kintecus.com.*, 2012.

5. Chuang, Y. H.; Parker, K. M.; Mitch, W. A., Development of Predictive Models for the Degradation of Halogenated Disinfection Byproducts during the UV/H_2O_2 Advanced Oxidation Process. *Environ. Sci. Technol.* **2016,** *50*, (20), 11209-11217.

6. Patton, S.; Li, W.; Couch, K. D.; Mezyk, S. P.; Ishida, K. P.; Liu, H., Impact of the Ultraviolet Photolysis of Monochloramine on 1,4-Dioxane Removal: New Insights into Potable Water Reuse. *Environ Sci Tech Let* **2017,** *4*, (1), 26-30.

7. Patton, S.; Romano, M.; Naddeo, V.; Ishida, K. P.; Liu, H., Photolysis of Mono- and Dichloramines in UV/Hydrogen Peroxide: Effects on 1,4-Dioxane Removal and Relevance in Water Reuse. *Environ Sci Technol* **2018,** *52*, (20), 11720-11727.

8. Laszlo, B.; Alfassi, Z. B.; Neta, P.; Huie, R. E., Kinetics and mechanism of the reaction of •NH2 with O_2 in aqueous solutions. *J Phys Chem A* **1998,** *102*, (44), 8498-8504.

9. Menkin, V. B.; Makarov, I. E.; Pikaev, A. K., Mechanism for Formation of Nitrite in Radiolysis of Aqueous-Solutions of Ammonia in the Presence of Oxygen. *High Energ Chem* **1991,** *25*, (1), 48-52.

10. Poskrebyshev, G. A.; Huie, R. E.; Neta, P., Radiolytic reactions of monochloramine in aqueous solutions. *J Phys Chem A* **2003,** *107*, (38), 7423-7428.

11. Seddon, W. A.; Fletcher, J. W.; Sopchyshyn, F.C., Pulse Radiolysis of Nitric Oxide in Aqueous Solution. *Can J Chem* **1973,** *51*, (7), 1123-1130.

12. NDRL/NIST Solution Kinetics Database. http://kinetics.nist.gov/solution/

13. Lewis, R. S.; Tannenbaum, S. R.; Deen, W. M., Kinetics of N-Nitrosation in Oxygenated Nitric-Oxide Solutions at Physiological pH - Role of Nitrous Anhydride and Effects of Phosphate and Chloride. *J Am Chem Soc* **1995,** *117*, (14), 3933-3939.

14. Mack, J.; Bolton, J. R., Photochemistry of nitrite and nitrate in aqueous solution: a review. *J Photoch Photobio A* **1999,** *128*, (1-3), 1-13.

15. Fisher, M. M.; Hamill, W. H. *Electronic processes in pulse-irradiated aqueous and alcoholic systems*; Univ. of Notre Dame, IN: 1973.

16. Buxton, G. V.; Bydder, M.; Salmon, G.A., The Reactivity Of Chlorine Atoms In Aqueous

Solution. *Transactions on Ecology and the Environment* **1999,** *35*, 699-702
17. Thomas, J., Rates of reaction of the hydroxyl radical. *Trans Faraday Soc* **1965,** *61*, 702-707.
18. Stephens, R. D., Absolute rate constants for the reaction of hydroxyl radicals with ammonia from 297 to 364 K. *J. Phys. Chem.* **1984,** *88*, (15), 3308-3313.
19. Gilbert, B. C.; Stell, J. K.; Peet, W. J.; Radford, K. J., Generation and reactions of the chlorine atom in aqueous solution. *Journal of the Chemical Society, Faraday Transactions 1: Physical Chemistry in Condensed Phases* **1988,** *84*, (10), 3319-3330.
20. Neta, P.; Schuler, R. H., Rate constants for the reaction of oxygen(1-) radicals with organic substrates in aqueous solution. *J. Phys. Chem.* **1975,** *79*, (1), 1-6.
21. Yang, Y.; Pignatello, J. J.; Ma, J.; Mitch, W. A., Effect of matrix components on UV/H_2O_2 and UV/$S_2O_8^{2-}$ advanced oxidation processes for trace organic degradation in reverse osmosis brines from municipal wastewater reuse facilities. *Water Res* **2016,** *89*, 192-200.
22. Buxton, G. V.; Greenstock, C. L.; Helman, W. P.; Ross, A. B., Critical review of rate constants for reactions of hydrated electrons, hydrogen atoms and hydroxyl radicals ($^{\cdot}OH/^{\cdot}O^{-}$) in aqueous solution. *J Phys Chem Ref Data* **1988,** *17*, (2), 513-886.
23. Crittenden, J. C.; Hu, S. M.; Hand, D. W.; Green, S. A., A kinetic model for H_2O_2/UV process in a completely mixed batch reactor. *Water Res* **1999,** *33*, (10), 2315-2328.
24. Buxton, G. V., Pulse radiolysis of aqueous solutions - Rate of reaction of OH with OH^-. *Trans Faraday Soc* **1970,** *66*, (571), 1656-1660.
25. Jayson, G. G.; Parsons, B. J.; Swallow, A. J., Some simple, highly reactive, inorganic chlorine derivatives in aqueous-solution - Their formation using pulses of radiation and their role in mechanism of fricke dosimeter. *J Chem Soc Farad Trans 1* **1973**, (9), 1597-1607.
26. McElroy, W. J., A Laser Photolysis Study of the Reaction of SO_4^- with Cl^- and the Subsequent Decay of Cl_2^- in Aqueous Solution. *J Phys Chem* **1990,** *94*, (6), 2435-2441.
27. Klaning, U. K.; Wolff, T., Laser flash-photolysis of HClO, ClO^-, HBrO, and BrO^- in aqueous-solution - Reactions of Cl-atoms and Br-atoms. *Ber Bunsen Phys Chem* **1985,** *89*, (3), 243-245.
28. Nagarajan, V.; Fessenden, R. W., Flash photolysis of transient radicals. 1. X_2- with X = Cl, Br, I, and SCN. *J. Phys. Chem.* **1985,** *89*, (11), 2330-2335.
29. Yu, X. Y.; Barker, J. R., Hydrogen peroxide photolysis in acidic aqueous solutions containing chloride ions. II. Quantum yield of $HO^{\cdot}_{(aq)}$ radicals. *J Phys Chem A* **2003,** *107*, (9), 1325-1332.
30. Grigorev, A. E.; Makarov, I. E.; Pikaev, A. K., Formation of Cl_2^- in the bulk solution during the radiolysis of concentrated aqueous-solutions of chlorides. *High Energ Chem* **1987,** *21*, (2), 99-102.
31. Wu, D.; Wong, D.; Dibartolo, B., Evolution of Cl_2^- in aqueous NaCl solutions. *J Photochem* **1980,** *14*, (4), 303-310.
32. Wagner, I.; Karthäuser, J.; Strehlow, H., On the decay of the dichloride anion Cl_2^- in aqueous solution. *Berichte der Bunsengesellschaft für physikalische Chemie* **1986,** *90*, (10), 861-867.
33. Matthew, B. M.; Anastasio, C., A chemical probe technique for the determination of reactive halogen species in aqueous solution: Part 1 - bromide solutions. *Atmos Chem Phys* **2006,** *6*, 2423-

2437.
34. Ershov, B. G., Kinetics, mechanism and intermediates of some radiation-induced reactions in aqueous solutions. *Russian Chemical Reviews* **2004,** *73*, (1), 101-113.
35. Bjergbakke, E.; Navaratnam, S.; Parsons, B. J.; Swallow, A. J., Reaction between HO_2 and chlorine in aqueous-solution. *J Am Chem Soc* **1981,** *103*, (19), 5926-5928.
36. Wang, T. X.; Margerum, D. W., Kinetics of Reversible Chlorine Hydrolysis - Temperature-Dependence and General Acid Base-Assisted Mechanisms. *Inorg Chem* **1994,** *33*, (6), 1050-1055.
37. Connick, R. E., The interaction of hydrogen peroxide and hypochlorous acid in acidic solutions containing chloride ion. *J Am Chem Soc* **1947,** *69*, (6), 1509-1514.
38. Long, C. A.; Bielski, B. H. J., Rate of reaction of superoxide radical with chloride-containing species. *J Phys Chem* **1980,** *84*, (5), 555-557.
39. Margerum, D. W.; Schurter, L. M.; Hobson, J.; Moore, E. E., Water Chlorination Chemistry - Nonmetal Redox Kinetics of Chloramine and Nitrite Ion. *Environ Sci Technol* **1994,** *28*, (2), 331-337.
40. Mezyk, S. P.; Helgeson, T.; Cole, S. K.; Cooper, W. J.; Fox, R. V.; Gardinali, P. R.; Mincher, B. J., Free radical chemistry of disinfection-byproducts. 1. Kinetics of hydrated electron and hydroxyl radical reactions with halonitromethanes in water. *J Phys Chem A* **2006,** *110*, (6), 2176-2180.
41. Haag, W. R.; Yao, C. C. D., Rate Constants for Reaction of Hydroxyl Radicals with Several Drinking Water Contaminants. *Environ Sci Technol* **1992,** *26*, (5), 1005-1013.
42. Lal, M.; Mahal, H. S., Reactions of Alkylbromides with Free Radicals in Aqueous Solutions. *Radiat Phys Chem* **1992,** *40*, (1), 23-26.
43. Sonntag, C.; von Gunten, U., *Chemistry of ozone in water and wastewater treatment: From basic principles to applications*. IWA publishing: 2012.
44. Dr. David Hokanson, Trussell Technologies, personal communication (September 25, 2017).
45. City of Santa Monica, CA, bid document comparison. https://www.smgov.net/departments/council/agendas/2011/20110628/s2011062803-K-1.pdf (retrieved November 9, 2018).
46. Mid American Regional Council, bid document comparison. http://www.marc.org/Government/Cooperative-Purchasing/pdf/BidTab_Chemicals65.aspx (retrieved November 9, 2018).
47. City of San Leandro, CA, bid document comparison. https://www.sanleandro.org/civicax/inc/blobfetch.aspx?BlobID=23488 (retrieved November 9, 2018).
48. City of Oxnard, CA, bid document comparison. https://www.oxnard.org/wp-content/uploads/2016/03/08.29.12_Bid_PW-13-1_Chemicals_Summary_2012.xls. (retrieved November 9, 2018).